Investigations on the Solution Architecture of Carboxylated Tamarind Seed Polysaccharide by Static and Dynamic Light Scattering

P. Lang,*,† K. Kajiwara,‡ and W. Burchard§

Iwan N. Stranski Institute for Physical and Theoretical Chemistry, Technical University, Strasse des 17, Juni 112, 1000 Berlin 12, Germany, Kyoto Institute of Technology, Matsugasaki, Sakyo-ku, Kyoto 606, Japan, and Institute for Macromolecular Chemistry, Stefan Meier Strasse 31, 7800 Freiburg, Germany

Received December 21, 1992; Revised Manuscript Received April 1, 1993

ABSTRACT: Carboxylated derivatives of tamarind seed polysaccharide with different degrees of derivatization have been synthesized by enzymatic oxidation of the galactose residues present in the native sample. The architecture of the derivatized polysaccharide in aqueous solution was investigated by static and dynamic light scattering. The angular distribution of the integrated scattering intensity, which can be well described by Koyama's theory, reveals a high degree of particle stiffness. Typical measures for the statistical Kuhn segment length are $l_K \geq 140$ nm. The experimental values for the mass per unit length, M_l, are typically 3–5 times higher than the one which is calculated from the primary structure of the polymer, indicating a structure of laterally aggregated polymer strands. This model is supported by the data from dynamic light scattering, which have been evaluated in terms of the Yamakawa–Fujii theory and the approach by Schmidt and Stockmayer. Both theories predict hydrodynamically effective cross-sectional diameters in the range of 8–15 nm. These values seem to be extremely high; however, they appear to be reasonable in comparison with data from other polysaccharides which have multistranded structures.

Introduction

Tamarind seed polysaccharide (TSP) is extracted from the seed kernels of the tamarind tree (*Tamarindus indica*), which grows mainly in Southeast Asia.[1] There have been numerous publications[2-4] in the past 30 years concerning the primary structure of TSP. There is general agreement about the nature of the backbone and the side chains. The polymer consists of a cellulose-type spine, which carries xylose and galactoxylose substituents. About 80% of the glucose residues are substituted by α 1→6 linked xylose units, which themselves are partially substituted by β 1→2 galactose residues. These structural units are displayed in Figure 1. The molar ratio of the monosaccharide residues is still subject to discussion.

Native TSP was shown to exhibit a strong tendency to self-aggregation[5,6] when dispersed in aqueous solvents. These aggregates consist of lateral assemblies of single polysaccharide strands, showing a behavior that could be well described by the wormlike chain[7] or the Kuhn[8] model. Static light scattering data on these particles shows that their stiffness is determined by the number of aggregated strands.

The tendency to aggregation can be increased to yield gelation or precipitation by addition of different low-molecular-weight species.[1,9] On the other hand, the contrary effect should be achieved by increasing either the quality of the solvent or the polarity of the solute. In the present study we have tested the second possibility, i.e., increasing the solubility by introduction of electrical charges into the polymer.

For the present investigation it was desirable to have available polymers with different number of charges per particle. For this purpose we have chosen the enzymatic oxidation of the galactose residues[10-12] as a tool to introduce charges. Since the degree of derivatization is determined by the enzyme incubation time,[13] the number of charges per particle may be easily adjusted to the desired value.

† Iwan N. Stranski Institute for Physical and Theoretical Chemistry.
‡ Kyoto Institute of Technology.
§ Institute for Macromolecular Chemistry.

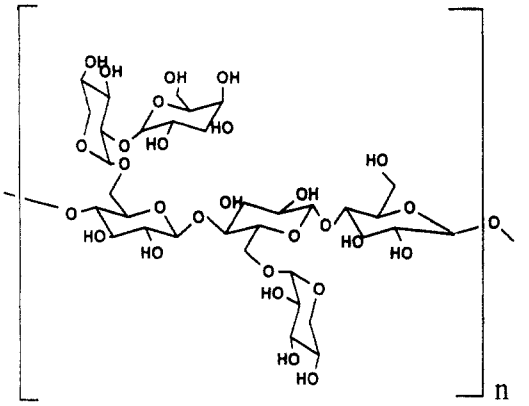

Figure 1. Average primary structure of tamarind seed polysaccharide. The cellulose type backbone is substituted by xylose(α 1→6) and galacto(β 1→2)xylose(α 1→6) residues. The molar ratio of monosaccharides is subject to discussion.

In comparison with the native polymer, we might expect the derivatives to show three possible effects. (i) The aggregates are split by the repulsive forces of the electrical charges, and therefore the particle stiffness decreases. (ii) The particles split, but the effect on the observed persistence length is overcompensated by the repulsion of the charges. (iii) The aggregates remain intact, and their stiffness increases because of the charges.

By intrinsic viscosity measurements, it has been shown previously that the particle stiffness of carboxylated and sulfated derivatives of TSP is increased with respect to the native polymer.[13] Thus the first possibility may be ruled out. For a distinction between the two remaining possibilities, it is necessary to measure the particle stiffness, which can be determined from static light scattering data.[14]

A direct measurement of the chain thickness is not possible by light scattering (LS) experiments. However, the mass per unit length M_l of a polymer can be calculated from static LS data, and the hydrodynamically effective cross-sectional diameter of a chain is available[15,16] from dynamic scattering measurements. Both quantities in

0024-9297/93/2226-3992$04.00/0

Table I. Enzyme Incubation Time and Resulting Degree of Derivatization for the Enzymatic Carboxylation of Tamarind Seed Polysaccharide[a]

sample	incub time (h)	deg of deriv (%)
TSPOX20	8	23
TSPOX50	20	47
TSPOX80	72	85

[a] The degree of oxidation was determined by potentiometric titration and calculated with respect to the polymer-bound galactose residues.

combination allow distinction between a single and a multistranded architecture.

Experimental Section

Native tamarind seed polysaccharide was obtained from Dai Nippon Pharmaceuticals Co. Ltd., Osaka, Japan. The commercial product was purified by spinning down insoluble parts for 30 min at $10^4 g$, followed by exhaustive dialysis against deionized water and final lyophilization. The efficiency of this simple procedure had been verified by an elaborate analysis, as described in ref 4.

The preparation of the carboxylated TSP sample (TSPOX) involves the enzymatic oxidation of the galactosyl C-6 hydroxymethyl groups to formyl groups.[10-12] To avoid product inhibition of the oxidizing enzyme, galactose oxidase, catalase has to be used as a coenzyme. The intermediate aldehydes are readily oxidized to carboxylate groups by alkaline I_2/I^- treatment. The experimental conditions were adjusted as follows.

To three 0.1% (w/v) aqueous solutions of purified TSP were added 0.6 mL of 0.1 M phosphate buffer (pH = 7.0; Merck, Darmstadt, Germany), 1200 units of catalase (E.C. 1.11.1.6) in 0.1 M phosphate buffer, and 2.2 units of galactose oxidase (E.C. 1.1.3.9) in the same solvent. Both enzymes were purchased from Sigma Chemical Co. and used without further purification. The reaction mixtures were kept at 27 °C for 8, 20, and 72 h, respectively, to yield extents of enzymatic reaction of about 25, 50, and 80% with respect to the galactose residues present in the native sample.

Subsequently 10 mg of iodine in 20 mM aqueous I_2/KI solution and 12 mg of sodium carbonate were added. The solutions were stirred at room temperature for 4 h and neutralized with 0.1 M HCl before heating them rapidly to 95 °C. After cooling down to ambient temperature, the solutions were filtered first through charcoal and then through 0.8-μm pore size filters. After addition of excess sodium chloride the solutions were dialyzed exhaustively against distilled water, carefully neutralized, and freeze-dried. All quantities quoted above are for 1 mg of galactose residue in the native sample. The actual degree of oxidation of the samples was quantified by potentiometric titration as described elsewhere.[12] The results are listed in Table I.

For light scattering measurements the carboxylated polymers were dissolved in aqueous sodium chloride. The resulting stock solutions were dialyzed against NaCl solutions of the same ionic strength under constant-volume conditions. The dilution for light scattering measurements was made with the solvent which had been used for the dialysis. Prior to measurements the solutions were filtered through 0.45-μm pore size filters directly into measuring cells. The light scattering measurements were performed at 25 °C on a commercial instrument (ALV Laservertriebsgesellschaft, Langen, Germany) which was equipped with an argon ion laser (λ = 488 nm) as a light source and an ALV 3000 structurator/correlator to record time autocorrelation functions of the scattered intensity.

All three samples were measured in 0.1 M sodium chloride solution. Additionally, the polymer with the highest degree of oxidation was investigated in aqueous solutions of different ionic strengths. Typical solution concentrations for the measurements were in the range of $2 \times 10^{-4} < c < 2 \times 10^{-3}$ g/mL.

Calculations for the particle scattering factor were carried out on an IBM 3090 computer in the computing center of the University of Freiburg. The occurring double integrals were evaluated numerically with routines from the Fortran IMSL library.

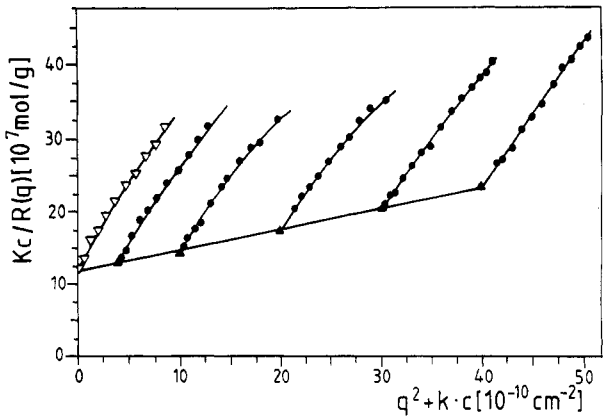

Figure 2. Zimm plot of the static light scattering data on TSPOX50 in 0.1 M NaCl aqueous solution. Polymer concentrations are 0.2×10^{-3}, 0.5×10^{-3}, 1.0×10^{-3}, 1.5×10^{-3}, and 2.0×10^{-3} g/mL. The open triangles represent extrapolated data at zero concentration.

Theoretical predictions for the hydrodynamic cross-sectional diameter were performed on an AsahiStellar work station (Stellar Computer Inc., Newton, MA) with homemade programs. For the required numerical integrations a Gaussian quadrature algorithm[17] was applied which had been tested for correct values of the hydrodynamic radius of Gaussian chains[18] and for the reproducibility of data from the literature.[19] Details of the mathematical expressions used for the calculations are summarized in Appendix A.

Results and Discussion

The primary light scattering data were analyzed by standard Zimm plot evaluation[20-22] according to the following familiar equations:

$$\frac{Kc}{R(q)} = \frac{1}{M_w}\left(1 + \frac{\langle S^2\rangle_z q^2}{3} + \ldots\right) + 2A_2 c + \ldots \quad (1)$$

$$D_{app} = D_z(1 + C\langle S^2\rangle_z q^2)(1 + k_D c) \quad (2)$$

where $R(q)$ is the ratio of scattered to incident intensity, q is the magnitude of the scattering vector $q = (4\pi/\lambda)\sin(\theta/2)$, θ is the scattering angle, K is the optical contrast factor, c is the polymer solution concentration, M_w is the weight-average molar mass, $\langle S^2\rangle_z$ is the z average of the mean square radius of gyration, A_2 is the second osmotic virial coefficient, D_{app} is the apparent diffusion coefficient, $D_{app} = \Gamma/q^2$, with Γ being the initial slope of the time autocorrelation function of the scattered field, D_{z0} is the z average of the translational diffusion coefficient, C is the architecture-dependent parameter, and k_D is the parameter describing the concentration dependence of the diffusion coefficient.

Static and dynamic Zimm plots as displayed in Figure 2 for one set of static data yielded the results which are listed in Table II. The hydrodynamic radii $1/R_h = \langle 1/R_H\rangle_z$, listed in the sixth column, were calculated from the translational diffusion coefficients with the Stokes–Einstein equation. The structure-sensitive parameter, ρ, in the last column is defined as the ratio of geometric radius of gyration and hydrodynamic radius, $\rho = R_g\langle 1/R_H\rangle_z$.

From the entries in Table II conclusions on the architecture of the particles can be drawn. The molar mass for TSPOX80 in solutions of different sodium chloride concentrations is not constant and is not related to the ionic strength of the solution. This observation may be interpreted as an indication that carboxylated TSP like the native polysaccharide forms aggregates randomly. This conclusion is consistent with the fact that the second

Table II. Weight-Average Molar Mass M_w, Radius of Gyration $R_g = \langle S^2 \rangle_z^{1/2}$, Second Osmotic Virial Coefficient A_2, z Average of the Hydrodynamic Radius R_h, and the Parameter $\rho = R_g/R_h$ for Carboxylated Tamarind Seed Polysaccharide As Determined by Light Scattering[a]

	c_{NaCl} (mol/L)	$M_w \times 10^{-6}$ (g/mol)	$A_2 \times 10^4$ ((mol·mL)/g^2)	R_g (nm)	R_h (nm)	ρ
TSPOX20	0.1	1.47	1.6	123	75	1.64
TSPOX50	0.1	0.85	2.4	83	55	1.51
TSPOX80	0.1	5.0	3.6	61	45	1.36
TSPOX80	0.01	0.79	3.8	95	58	1.98
TSPOX80	10^{-3}	0.56	4.0	71	41	1.73
TSP		1.16	7.0	122	78	1.56
gellan	0.1	0.43	22.0	159	52	3.06
xanthan	0.1	2.94	4.9	290	137	2.12
TA1-EPS	0.1	1.29	6.9	127	69	1.84

[a] The entries in the second column are the concentration of NaCl in mol/L in the solvent. The data of native TSP are added for comparison. Data of gellan, xanthan, and TA1-EPS were taken from ref 32.

Table III. Contour Length L_c, Kuhn Segment Length l_K, Polydispersity $U = M_w/M_n$, and Mass per Unit Length M_l of Carboxylated and Native TSP[a]

	c_{NaCl} (mol/L)	L_c (nm)	N_K	l_K (nm)	U	M_l (g/(mol·nm))	R_g(th) (nm)
TSPOX20	0.1	532	3.8	140	2.0	2763	121.4
TSPOX50	0.1	283	2.3	123	3.0	3003	83.6
TSPOX80	0.1	226	1.3	174	1.3	2212	63.4
TSPOX80	0.01	327	0.5	654	1.1	2422	95.4
TSPOX80	10^{-3}	180	0.6	300	2.0	3127	71.2
TSP		573	3.4	107	1.5	2100	127

[a] The parameters gave the best agreement of theoretical predictions for the particle scattering factor according to the Koyama theory with experimental data. The theoretical value of R_g(th), listed in column eight, was calculated by use of eq 5.

virial coefficients A_2 (regarded as a measure for the solvent quality or the solubility of the polymer) of the carboxylated samples and the native TSP are not significantly different.

The ρ parameters are generally higher than the experimental values[23] for unperturbed, monodisperse Gaussian chains, thus indicating a stretched linear architecture and a nonnegligible polydispersity.

The angular distribution of the intensity scattered by particles in solution is usually described by the particle scattering factor $P(q)$. For polydisperse wormlike chains, i.e., semiflexible linear particles, $P(q)$ contains information on the polydispersity and the chain stiffness of the investigated material.

If the particle scattering factor, which in terms of experimentally accessible data reads

$$P(q) = \left(\frac{R(q)}{KcM_w}\right)_{c=0} \tag{3}$$

is plotted as $qP(q)/\pi$ versus $u = R_g q$ (Casassa–Holtzer[24,25] plot), the following parameters are obtained.[14]

(i) The position of the maximum in the curve is related to the polydispersity index $U = M_w/M_n$.

(ii) The ratio of the height of the maximum to the final plateau value at large q is a measure of the reciprocal of the statistical Kuhn segment length l_K.

(iii) The plateau value is the reciprocal of the contour length L_c.

Because of the limited range of accessible scattering vectors, in the present case it was not possible to extract the whole set of information from the experimental data alone. Therefore, we carried out a least-squares fit with theoretical curves for the particle scattering factor, using

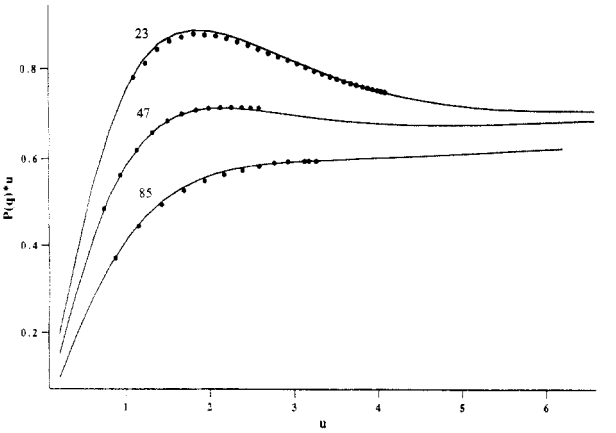

Figure 3. Casassa–Holtzer plot for carboxylated TSP samples with different degrees of derivation as indicated by the numbers. The full lines are theoretical curves calculated according to the Koyama theory with the values from Table III.

the expression given by Koyama[26]

$$P(q) = \frac{2}{L_c^2}\int_0^{L_c}(L_c - t)\varphi(q)\,dt \tag{4}$$

Details of the function $\varphi(q)$ are given in the Appendix. Since the investigated samples were not monodisperse, the expression in eq 4 was modified for polydisperse systems by assuming a Schulz–Zimm[20,27] type distribution of the contour length. The theoretical predictions were calculated for different sets of the parameters l_K, L_c, and U and compared with the experimental data. The combinations which yielded the best fit are listed in Table III. To make sure that these combinations are physically meaningful, it was checked that they produce the experimental value of the radius of gyration, as given by the formula by Benoit and Doty,[19,29] for polydisperse wormlike chains.

$$\langle S^2 \rangle_z = l_K\frac{k+2}{6y} - \frac{l_K^2}{4} + \frac{l_K^3}{4L_w} - \frac{l_K^4}{8k(k+1)}\left[y^2 - \frac{y^{k+2}}{y + 2/l_K}\right] \tag{5}$$

$$y = (k+1)/L_w$$

Here, $k = (U-1)^{-1}$ and L_w is the weight-average of the contour length.

A Casassa–Holtzer plot of the experimental data from all three samples in 0.1 M NaCl solution, together with the best theoretical approximations, is displayed in Figure 3. As expected, the particle stiffness, which is represented by the reciprocal ratio of maximum height to plateau value, increases with the percentage of derivatization.

Contrary to the particle stiffness, the final plateau values in the Casassa–Holtzer plot are correlated neither to the degree of oxidation nor to the ionic strength of the solvent. The final plateau of this plot gives the reciprocal of the weight average of the contour length. Thus it is possible to obtain the absolute value of the mass per unit length $M_l = M_w/L_{cw} = M/L$, without further corrections for polydispersity.[25] In the present case, the estimated values for the mass per unit length all lie in the range of about 2100–3200 g/(mol·nm). A theoretical value for the linear mass density M_l of a single-stranded TSPOX chain can be estimated which depends to a certain degree on the assumed primary structure.[2-4] However, this theoretically expected value for M_l lies in the range of 600–700 g/(mol·nm) and is therefore 3–5 times lower than the

experimentally detected values. This behavior shows that the present particles consist of multistranded aggregates. Similar observations had been made on native TSP,[5,6] as seen from the corresponding entry in Table III.

The number of Kuhn segments per contour length N_K, which is also listed in Table III, shows that the particle stiffness increases with the degree of derivatization, as expected. Native samples of TSP which are aggregated to the same extent have only slightly smaller Kuhn segment lengths. The segment length of a single strand of TSP was estimated[5] to be $l_K \approx 30$ nm.

From these findings we may reach two conclusions: (i) The observed particle stiffness of carboxylated TSP is caused mainly by the occurrence of multistranded lateral aggregates, similar to those in native TSP. The repulsive forces due to the introduction of charges onto the polymer make only a minor contribution to the particle stiffness. (ii) The tendency of TSP to self-aggregation is too strong to be overcome by electrostatic repulsive forces.

The occurrence of multistranded aggregates should be detectable also by their hydrodynamic properties. Especially the hydrodynamically effective cross-sectional diameter of the particles should have unusually high values.

From the z-average translational diffusion coefficient D_z, which is measurable in dynamic light scattering, a hydrodynamically effective radius R_h can be calculated from the Stokes–Einstein relationship,

$$R_h = \frac{k_B T}{6\pi\eta_0 D_z} \tag{6}$$

where k_B is the Boltzmann constant, T is the absolute temperature, and η_0 is the viscosity of the solvent.

The Yamakawa–Fujii theory[15] and the Schmidt–Stockmayer approach[16] describe the hydrodynamic radius R_H of wormlike chains as a function of the contour length, the Kuhn segment length, and the chain diameter. The Yamakawa–Fujii treatment is based on the calculations of the hydrodynamic properties of a random coil and a rigid rod, respectively, and the assumption of a smooth transition between these two cases. Thus two different expressions for the hydrodynamic radius are given, which apply for different regimes of the contour length.

$$\frac{1}{R_H} = 2\sum_{i=1}^{5} A_i L_r^{-i/2} \qquad \text{for } L_r < 2.278 \tag{7}$$

$$\frac{1}{R_H} = \frac{2}{L_r}\left[C_1 \ln\left(\frac{L_r}{d_r}\right) + C_2 + C_3 L_r + C_4 L_r^2 + C_5 L_r^3 + \ldots\right] \qquad \text{for } L_r \geq 2.278 \tag{8}$$

The coefficients A_i and C_i are polynomials of the reduced chain diameter d_r, which are given in the Appendix, and L_r is the reduced contour length, $L_r = L_c/l_K$ ($=N_K$).

Schmidt and Stockmayer, on the other hand, calculated the hydrodynamic radius of a wormlike chain, using the moments of the distribution function as given by Koyama, which in the following equation appear as the parameters A and B.

$$\frac{1}{R_H} = \frac{2}{L_c^2}\int_0^{L_c}(L_c - s)B^{-1}\,\mathrm{erf}\left(\frac{B}{2A}\right)ds \tag{9}$$

The parameter s is usually substituted by $(d^2/4 + s^2)^{1/2}$, where d plays the role of an effective diameter. Details on A and B are also given in the Appendix.

If we assume the values of contour length, polydispersity, and segment length as given in Table III to be correct, there remains only the chain diameter as a variable quantity in eqs 7–9. Thus, it becomes possible to estimate the chain diameter by calculating theoretical values of the hydrodynamic radius as a function of the cross-sectional diameter and comparing the results with the experimental data. For this purpose also the expressions in eqs 7–9 have to be modified for polydisperse systems, which again yields integrals that must be evaluated numerically. The values of d which are listed in Table IV gave the best agreement of the hydrodynamic radii calculated by this procedure with the experimental data.

With eqs 5 and 7–9 it becomes possible to calculate the ρ parameter of wormlike chains as a function of the chain diameter. In Figure 4 the theoretically predicted dependence of the ρ parameter is displayed for different axial ratios L_c/d. Both theories give qualitatively similar results, but the Yamakawa–Fujii theory predicts slightly lower values of R_h and thus higher values of ρ.

From Figure 4 it is evident that the ρ parameter of chains with a low number of Kuhn segments decreases strongly if the cross-section increases. This may explain the relatively low ρ values of native and carboxylated TSP as compared with other systems of high stiffness.[29] On the other hand, the theoretical curve for an axial ratio of $L_c/d = 18$ fits the data reasonably well, which is in good agreement with corresponding data on poly(benzyl glutamate) in dimethylformamide,[19] which is reported to have $L_c/d \approx 20$. This value also coincides with the axial ratio of polystyrene with less than about 100 segments.[30,31] However, despite these apparent agreements, the absolute values of the chain diameter of carboxylated TSP are extremely high, as can be seen from Table IV. The data given by the Yamakawa–Fujii treatment are even higher than the ones from the Schmidt–Stockmayer theory. This

Table IV. Hydrodynamically Effective Diameter of the Cross-Section for Various Polysaccharides[a]

	c_{NaCl} (mol/L)	R_h (nm)	d_{SS} (nm)	d_{YF} (nm)
TSPOX20	0.1	75	17.5	24.0
TSPOX50	0.1	55	17	25.5
TSPOX80	0.1	46	15.5	28.5
TSPOX80	0.01	58	8.5	15
TSPOX80	10^{-3}	41	12.5	19
TSP		78	17	24
gellan	0.1	52	2	2
xanthan	0.1	137	8.5	16
TA1-EPS	0.1	69	15	21

[a] The listed values gave the best agreement between experimental data and the predictions according to the Yamakawa–Fujii (d_{YF}) and Schmidt–Stockmayer (d_{SS}) approximations.

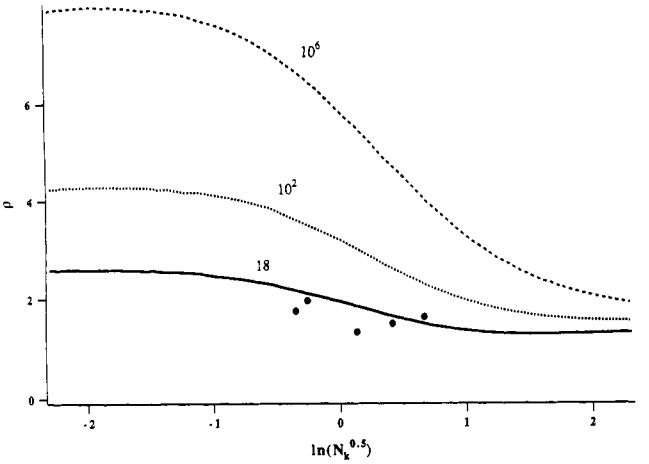

Figure 4. Theoretical predictions for the dependence of the ρ parameter on the chain length for different diameters. The curves are calculated for different axial ratios L_c/d, which are indicated by the numbers. The experimental data on carboxylated TSP are represented by the dots.

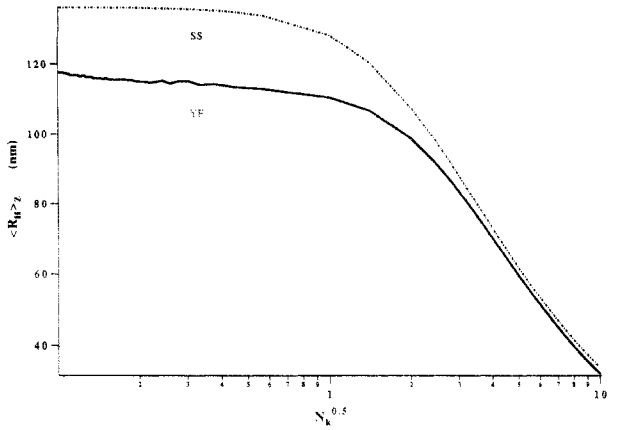

Figure 5. Theoretical prediction for the dependence of the z average of the hydrodynamic radius $R_h = ((1/R_H)_z)^{-1}$ of a polydisperse wormlike polymer on the chain stiffness according to Yamakawa and Fujii (YF) and Schmidt and Stockmayer (SS). Both curves were calculated with fixed contour length $N_K = 1000$ nm, axial ratio $L_c/d = 100$, and polydispersity $U = 2$, varying the Kuhn segment length in the range $10 < l_K < 10^5$ nm.

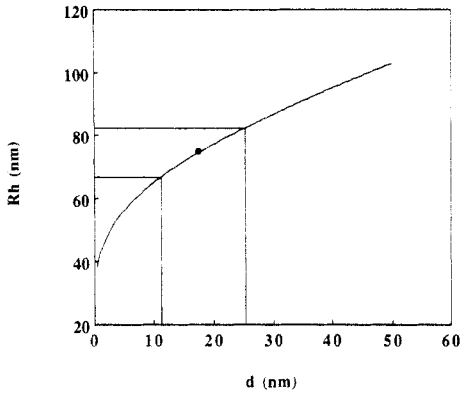

Figure 6. Dependence of the hydrodynamic radius, as calculated by use of eqs 7–9 on the cross-sectional diameter of the chain. The curve was calculated using the contour length, segment length, and polydispersity of TSPOX20. The dot is the experimentally determined value of R_h. The horizontal bars represent the experimental error, and the vertical bars define the resulting error in the estimation of the cross-sectional diameter.

fact is also reflected in Figure 5, from which it is evident that in the range $0 < N_K < 4$ the differences in the predictions of the two theories are quite substantial. This may result from the assumption in the Yamakawa–Fujii approximation that the transition from rigid rod to coil behavior remains unaltered at $N_K = 2.278$, irrespectively of the chain thickness, as long as the axial ratio is large enough. This simplification may not be valid for the samples investigated in the present work.

To understand the extremely high values of the particle cross-sectional diameters, we first have to consider experimental errors. The reproducibility of dynamic light scattering data lies in the range of ±5% for systems which are easy to handle. Another source for large errors is the possible presence of small amounts of highly aggregated particles. One can easily estimate that the presence of only 2% particles of double average size will increase the z average of the measure by about 10%. These errors can lead to an overestimation of the cross-sectional diameter by a factor of 2, as is illustrated in Figure 6.

In view of these considerations, the comparison of the present data on carboxylated TSP with experimental values reported for polysaccharides with multistranded conformations[32] gives at least qualitative agreement. The hydrodynamic data on gellan in a double-helical conformation gave a very low value for the chain diameter, but the double helix of xanthan and the triple helix of TA1-EPS, which both have bulky side groups like TSP, have hydrodynamically effective cross-sectional diameters which match perfectly with the data on carboxylated and native TSP (see corresponding entries in Table IV).

However, cross-sectional diameters in the range of about 10 nm are difficult to imagine even for multistranded structures. An intuitive explanation is given by the following speculative model. If the bundles (or helices) were frayed out at the ends, the hydrodynamic hindrance would be markedly increased as compared to a particle where the strands are closely packed along the entire contour length. The hydrodynamically effective shape of such particles might better be described by a long dumbbell (with a semiflexible bar) than by a skipping rope.

Conclusions

The static and dynamic light scattering data on carboxylated TSP can be well described by the wormlike chain model. However, theoretical predictions and experimental data will match only if one allows for extremely high values of the linear mass densities and the hydrodynamically effective diameters of the cross-section. This behavior had been reported also for native TSP; thus, it seems likely that the solution architecture of the carboxylated sample is similar to that of native TSP, i.e., bundle-shaped lateral aggregates of single polymer strands. The introduction of electrical charges, which very likely is a derivatization of aggregates already present, does not significantly influence the solubility of the polysaccharide. This shows that the tendency to aggregation of TSP, either carboxylated or native, is very high and that the solution properties of these samples are determined by aggregates and not by single polymer strands. In recent years such behavior has been reported quite frequently for different polysaccharides in aqueous solution, indicating that water is only a marginal solvent for polysaccharides. Also, highly derivatized polysaccharides have been reported to be not well molecularly dispersed in solvents. It is thus quite tempting to believe that forming insoluble aggregates is a natural feature of polysaccharides and that this fact should be accounted for in future investigations.

Acknowledgment. The experimental parts of this study were carried out at the Institute for Macromolecular Chemistry, Freiburg, Germany. The calculations were performed mainly during P.L.'s stay at the Kyoto Institute of Technology, Kyoto, Japan. Both institutes are thanked for the use of their facilities. P.L. thanks the Japan Society for the Promotion of Science (JSPS) for financial support and the Alexander von Humboldt Stiftung for a Feodor Lynen Fellowship.

Appendix A

The Koyama Theory.[26] In Koyama's notation the particle scattering factor for any kind of linear polymer reads

$$P(q) = \frac{2}{L_c^2}\int_0^{L_c}(L_c - t)\varphi(q)\,dt \qquad \text{(A1)}$$

where $\varphi(q)$ is the Fourier transform of the distance distribution function of scatterers within the particle averaged for all orientations of the scattering vector. It is assumed that the function $\varphi(q)$ for wormlike chains may be derived from a hybrid of the two functions describing

the limiting cases of a random coil and a rigid rod.

$$\Phi(q,\psi) = \exp\left(-\frac{u^2}{3}xf(x) + iu\cos\psi\, xg(x)\right) \quad \text{(A2)}$$

where ψ is the angle between a chain segment and the scattering vector, u is the product of the segment length l_K and the scattering vector q, x denotes the number of segments per contour length, and the functions $f(x)$ and $g(x)$ are defined for the hybridization. Averaging over all values of ψ yields

$$\varphi(q) = \exp\left(-\frac{u^2}{3}xf(x)\right)\frac{\sin(u\, xg(x))}{u\, xg(x)} \quad \text{(A3)}$$

Thus the particle scattering factor is

$$P(q) = \frac{2}{L_c^2}\int_0^{L_c}(L_c - t)\frac{\sin(q\, tg(t))}{q\, tg(t)}\exp\left(-\frac{q^2 l_K}{6}tf(t)\right) dt \quad \text{(A4)}$$

with t being a contour distance, $t = xl_K/2$. The functions $f(t)$ and $g(t)$ are given as

$$tf(t) = \frac{\langle r^2\rangle}{l_K}\left[1 - \frac{10^{1/2}}{2}\left(1 - \frac{3K}{5}\right)^{1/2}\right] \quad \text{(A5)}$$

$$tg(t) = \frac{\langle r^2\rangle}{2}\left[\frac{5}{2}\left(1 - \frac{3K}{5}\right)\right]^{1/2} \quad \text{(A6)}$$

Here, $K = \langle r^4\rangle/\langle r^2\rangle^2$, where the expressions in angular brackets denote the second and fourth moments of the end-to-end distance distribution function, which are given as

$$\langle r^2\rangle = l_K t - \frac{l_K}{2}(1 - E) \quad \text{(A7)}$$

$$\langle r^4\rangle = l_K^2\left(\frac{5t^2}{3} - \frac{26tl_K}{9} - \frac{l_K^2(1-E)}{54} + 2l_K^2(1-E) + t + l_K E\right) \quad \text{(A8)}$$

with $E = \exp(-2t/l_K)$.

The Yamakawa–Fujii Theory.[15] Originally, Yamakawa and Fujii calculated the sedimentation coefficient of a wormlike cylinder. Their treatment can be easily applied to the calculation of the hydrodynamic radius, simply by using the Stokes relation. Their expression for R_H reads then

$$\frac{1}{R_H} = \frac{2}{L_r^2}\int_0^{L_r}(L_r - t)K(t)\, dt \quad \text{(A9)}$$

While t is the distance between two points on the cylinder axis, the kernel $K(t)$ of the integral in eq A9 is, according to its definition, the mean distance between a point on the cylinder axis and one on the surface. Therefore, the hydrodynamic radius is dependent on the diameter of the cylinder d. However, the prediction of $K(t)$ is not possible exactly; therefore Yamakawa and Fujii used the expressions for the limiting cases of zero t and infinite t to calculate their approximation.

$$\lim_{t\to 0} K = (t^2 + a^2)^{1/2} \quad \text{(A10)}$$

$$\lim_{t\to\infty} K = \left(\frac{6}{\pi t}\right)^{1/2}\left(1 - \frac{1 + 20a^2}{40t} - \frac{1/73 - 1176a^2 - 1008a^4}{4480t^2} + \ldots\right) \quad \text{(A11)}$$

where a is the radius of the cylinder, $a = d/2$. A smooth transition between these two cases is produced by the condition that at their intersect $t = \sigma$ both expressions and also their first and second derivatives shall give the same value. With this approximation the final expressions for the hydrodynamic radius read

$$\frac{1}{R_H} = 2\sum_{i=1}^{5} A_i L_r^{-i/2} \quad \text{for } L_r < 2.278 \quad \text{(A12)}$$

$$\frac{1}{R_H} = \frac{2}{L_r}\left[C_1\ln\left(\frac{L_r}{d_r}\right) + C_2 + C_3 L_r + C_4 L_r^2 + C_5 L_r^3 + C_6\frac{d_r}{L_r}\ln\left(\frac{L_r}{d_r}\right) + \sum_{i=1}^{4} C_{i+6}\left(\frac{d_r}{L_r}\right)^i\right] \quad \text{for } L_r \geq 2.278 \quad \text{(A13)}$$

The coefficients A_i and C_i are polynomials in the diameter. For the numerical values the reader is referred to the original paper.[15]

The Schmidt–Stockmayer Theory.[16] This approach is based on the theoretical expression for the so-called first cumulant $\Gamma(q)$ in dynamic light scattering which had been given by Akcasu and Gurol.[33] Tanaka and Stockmayer gave a relation for the hydrodynamic radius[34] which is consistent with Kirkwoods approximation for the translational diffusion coefficient.[35]

$$\frac{1}{R_H} = \frac{2}{L_c^2}\int_0^{L_c}(L_c - s)\langle r(s)^{-1}\rangle\, ds \quad \text{(A14)}$$

with

$$\langle r(s)^{-1}\rangle = \int_0^\infty \frac{1}{R} W(r,s)\, d^3r$$

Here, r is the distance between two points on a chain separated by the contour length s, and $W(r,s)$ is the corresponding distribution function. Using Koyama's approximation for the latter, Schmidt and Stockmayer resolved the second integral in eq A14 analytically.

$$\langle r(s)^{-1}\rangle = B^{-1}\,\mathrm{erf}\left(\frac{B}{2A}\right) \quad \text{(A15)}$$

with

$$A^2 = \langle r^2\rangle\frac{1-\eta}{6} \qquad B^2 = \eta\langle r^2\rangle$$

$$\eta = \left[\frac{1}{2}\left(5 - \frac{3\langle r^4\rangle}{\langle r^2\rangle^2}\right)\right]^{1/2}$$

Here, the $\langle r^i\rangle$ are the moments of the end-to-end distance distribution function as given by Koyama. Introducing eq A15 into eq A14 yields the following expression for the hydrodynamic radius.

$$\frac{1}{R_H} = \frac{2}{L_c^2}\int_0^{L_c}(L_c - s)B^{-1}\,\mathrm{erf}\left(\frac{B}{2A}\right) ds \quad \text{(A16)}$$

References and Notes

(1) Gerard, T. In *Handbook of Water Soluble Gums and Resins*; Davidson, R. L., Ed.; McGraw-Hill: New York, 1980.
(2) Srivastava, H. C.; Singh, P. P. *Carbohydr. Res.* **1967**, *4*, 326.
(3) Kooiman, P. *Recl. Trav. Chim. Pays-Bas* **1971**, *80*, 849.
(4) Gidley, M. J.; Lillford, P. J.; Rowlands, D. W.; Lang, P.; Dentini, M.; Crescenzi, V.; Edward, S. M.; Fanutti, C.; Reed, J. S. G. *Carbohydr. Res.* **1991**, *214*, 299 and references quoted therein.
(5) Lang, P.; Burchard, W. *Makromol. Chem.*, submitted.
(6) Lang, P.; Kajiwara, K. *Int. J. Biomater. Sci.*, in press.
(7) Kratky, O.; Porod, G. *Recl. Trav. Chim. Pays-Bas* **1949**, *68*, 1106.
(8) Kuhn, W. *Kolloid Z.* **1934**, *68*, 2.
(9) Lang, P.; Burchard, W. *Macromolecules* **1991**, *24*, 814.
(10) Hall, L. D.; Yalpani, M. *Carbohydr. Res.* **1980**, *81*, C10.

(11) Rogers, J. K.; Thompson, M. S. *Carbohydr. Res.* **1968**, *7*, 66.
(12) Dentini, M.; Crescenzi, V. *Carbohydr. Polym.* **1986**, *6*, 493.
(13) Lang, P.; Masci, G.; Dentini, M.; Crescenzi, V.; Cooke, D.; Gidley, M. J.; Fanutti, C.; Reed, J. S. G. *Carbohydr. Polym.* **1992**, *17*, 185.
(14) Schmidt, M.; Burchard, W.; Pradossi, G. *Makromol. Chem., Rapid Commun.* **1985**, *6*, 767.
(15) Yamakawa, H.; Fujii, M. *Macromolecules* **1973**, *6*, 407.
(16) Schmidt, M.; Stockmayer, W. H. *Macromolecules* **1984**, *17*, 509.
(17) Press, W. H.; Flannery, B. P.; Teuckolsky, S. A.; Vettering, W. K. *Numerical Recipes, The Art of Scientific Computing*; Cambridge University Press: Cambridge, 1986.
(18) Kirkwood, J. G.; Riseman, J. *J. Chem. Phys.* **1948**, *16*, 565.
(19) Schmidt, M. *Macromolecules* **1984**, *17*, 553.
(20) Zimm, B. H. *J. Chem. Phys.* **1948**, *16*, 1099.
(21) Berry, G. C. *J. Chem. Phys.* **1966**, *44*, 4550.
(22) Burchard, W. *Makromol. Chem., Macromol. Symp.* **1988**, *18*, 1.
(23) Schmidt, M.; Burchard, W. *Macromolecules* **1981**, *14*, 210.
(24) Casassa, E. F. *J. Chem. Phys.* **1955**, *23*, 596.
(25) Holtzer, A. *J. Polym. Sci.* **1955**, *17*, 432.
(26) Koyama, R. *J. Phys. Soc. Jpn.* **1973**, *34*, 1029.
(27) Schulz, G. V. *Z. Phys. Chem.* **1939**, *B43*, 25.
(28) Benoit, H.; Doty, P. *J. Phys. Chem.* **1953**, *57*, 958.
(29) Denkinger, P.; Burchard, W.; Kunz, M. *J. Phys. Chem.* **1989**, *93*, 1428.
(30) Huber, K.; Burchard, W.; Akcasu, A. *Z. Macromolecules* **1985**, *18*, 2743.
(31) Koyama, H.; Yoshizaki, T.; Einaga, Y.; Yamakawa, H. *Macromolecules* **1991**, *24*, 932.
(32) Dentini, M.; Coviello, T.; Burchard, W.; Crescenzi, V. *Macromolecules* **1988**, *21*, 3312.
(33) Akcasu, A. Z.; Gurol, H. *J. Polym. Sci., Polym. Phys. Ed.* **1976**, *14*, 1.
(34) Tanaka, G.; Stockmayer, W. H. *Proc. Natl. Acad. Sci. U.S.A.* **1982**, *79*, 6401.
(35) Kirkwood, J. G. *J. Polym. Sci.* **1954**, *12*, 1.